Line optical tweezers instrument for measuring nanoscale interactions and kinetics

Paul L. Biancaniello
Department of Physics and Astronomy, University of Pennsylvania, Philadelphia, Pennsylvania 19104

John C. Crocker
Department of Chemical and Biomolecular Engineering, University of Pennsylvania, Philadelphia, Pennsylvania 19104

(Received 23 June 2006; accepted 9 October 2006; published online 15 November 2006)

We describe an optical tweezers instrument for measuring short-ranged colloidal interactions, based on a combination of a continuous wave line optical tweezers, high speed video microscopy, and laser illumination. Our implementation can measure the separation of two nearly contacting microspheres to better than 4 nm at rates in excess of 10 kHz. A simple image analysis algorithm allows us to sensibly remove effects from diffraction blurring and microsphere image overlap for separations ranging from contact to at least 100 nm. The result is a versatile instrument for measuring steric, chemical and single-molecular interactions and dynamics, with a force resolution significantly better than achievable with current atomic force microscopy. We demonstrate the effectiveness of the instrument with measurements of the pair interactions and dynamics of microspheres in the presence of transient molecular bridges of DNA or surfactant micelles. © *2006 American Institute of Physics.* [DOI: 10.1063/1.2387893]

INTRODUCTION

Optical tweezers are a noninvasive way to manipulate fluid suspended microscopic objects in three dimensions using a single laser beam focused by a microscope objective.[1] For their ability to easily measure piconewton forces and subnanometer motions of micron-sized objects, tweezers have been widely adopted for the study of single-molecular motor sliding motility. Our goal here is to describe the design and operating principles of a line optical tweezers (LOT) instrument for the study of colloidal and surface forces. Such small forces have also been studied using the surface force apparatus (SFA), atomic force microscopy (AFM), total internal reflection microscopy (TIRM), and reflection interference microscopy (RIM). While all these methods excel in different applications, the LOT approach has several unique advantages, including exquisite force resolution, small probe size, and the use of two colloidal surfaces rather than flat "model" surfaces. The primary limitation of earlier LOT measurements was poor resolution, both spatially (typically 15–50 nm) and temporally (video rate, 17 ms), which limited them to the study of long-ranged colloidal interactions. We will describe the improvements which allow the study of nanoscale interactions and molecular binding kinetics using a LOT with a 4 nm resolution for particle separation and a temporal resolution of 10 μs. We demonstrate the utility of this instrument by studying the short-ranged interactions and binding kinetics of two microspheres pulled together by DNA bridges or surfactant micelles.

The first LOT was demonstrated by Sasaki *et al.*[2] By rapidly scanning a conventional (point) optical tweezers along a curve in the specimen plane they formed a trap that could hold colloidal microspheres on a one-dimensional curve in three-dimensional space. The relative trapping strength (depth) of the trap at different points on the curve depends on the time-averaged intensity and beam alignment, which may be controlled by scan rate, external modulation, or intentional misalignment. To date, LOTs have been used to construct thermal ratchets,[3] perform colloidal interaction measurements,[4–8] and produce passive "force clamps" (constant lateral force traps) for single molecule biophysics assays.[9] These traps were formed variously by scanning the laser using rotating mirrors,[3,10] galvanometer-driven mirrors,[2,5] or acousto-optical deflectors.[11] One-dimensional arrays of particles have also been trapped in the counterpropagating Gaussian beams of fiber optic traps.[12] Recently, similar, unscanned circular and clover-leaf shaped traps[13] and uniform line optical traps[14] have been formed using holographic optical tweezers (HOT) methods.

METHODS

Line optical tweezers

For its simplicity, optical efficiency and strong particle confinement to the focal plane, we chose a continuous wave (cw) line optical tweezers.[5] We use a high-power, single-mode collimated diode laser source (~100 mW, $\lambda = 830$ nm, beam diameter ~7 mm; Melles-Griot, model 56ICS115) and an inverted optical microscope (DM-IRB, Leica) with an oil-immersion microscope objective (Plan-Apo, 100X, numerical aperture, NA=1.4; Leica). Our optical train [Fig. 1(a)] consists of three Keplerian telescopes, two using spherical lenses and one using cylindical lenses. The design goal is to apply a large, adjustable anamorphic magnification (20–30×) to a Gaussian beam without introducing a significant amount of astigmatism or spherical aberration. By sig-

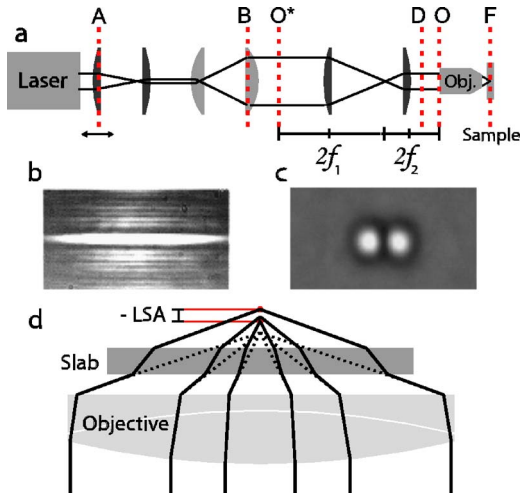

FIG. 1. (Color online) (a) Schematic of optical train for the line optical trap. The first and last pairs of lenses (dark grey) are planoconvex spherical lenses where as the middle pair (light gray) are planoconvex cylindrical lenses, all mounted outside an inverted optical microscope. The first two telescopes give the laser an anamorphic magnification of $\approx 20\times$ at point B, without adding astigmatism. The third telescope projects the objective back aperture O, to an external plane O^* (through an arc illuminator alignment port) where we place a steering mirror (not shown). The separation of O and O^* is twice the sum of lens' focal lengths f_1+f_2. D is the position of our imaging IR dichroic, mounted on a modified epifluorescence filter cube within the microscope body, which reflects the horizontal trapping beam vertically into the objective, while transmitting imaging light. (b) and (c) show the laser line created at F and two trapped microspheres, respectively, with the latter enlarged about $2\times$. (d) illustrates LSA generation by a refractive slab.

nificantly narrowing the beam in one dimension at objective's back aperture, we create a long "line" focus in the specimen plane with a Gaussian intensity profile along its length. Because we are under filling the back aperture in that direction, there is no beam truncation, resulting in a smooth, ripple-free Gaussian profile along the line in the specimen plane.

The first telescope in our optical train [Fig. 1(a)] simply reduces the diameter of our Gaussian laser beam. As we will discuss later, the small diameter of the beam waist projected by the first telescope (at the plane B) ultimately determines the line length generated in the specimen plane. Next, a cylindrical lens telescope enlarges the beam in one direction. In our implementation, the beam at the plane B has a small diameter of about 0.75 mm and a large diameter of 15 mm in the perpendicular direction. The third telescope reduces this beam in size and projects it into the microscope body, off a 45° dichroic and onto objective's back aperture. This lens pair also creates a conjugate plane O^* to the back aperture of the objective O. As is commonly done with point optical tweezers, a steering mirror at this conjugate point allows the trap to be centered in the objective's field of view during alignment while minimizing vignetting of the beam at the objective.

The length of the line focus in the specimen plane [shown in Fig. 1(b)] is inversely proportional to the narrow width of the beam entering the back aperture. We adjust the beam diameter by translating the first lens (plane A) of the first telescope along the optical axis. To achieve zero astigmatism in this arrangement, the first telescope is first focused to project a diffraction-limited beam waist at B (in the plane where the cylindrical telescope is optically neutral). Refocusing the cylindrical telescope until its exit beam is also collimated at B (in the perpendicular plane) then nulls the astigmatism. Small translations of the first lens (at A) then increase the small beam diameter at B and O^* and correspondingly decrease the length of the line focus in the sample plane F (which is a Fourier plane for O^*). The small amount of astigmatism introduced by this adjustment does not appear to aversely affect trapping ability. Since the force exerted on a trapped object in an optical tweezers is proportional to the gradient of the intensity, trapped microspheres feel a harmonic force near the trap center with a spring constant that is inversely proportional to the length of the line trap. Adjusting the trap's spring constant along the line will prove useful for nulling the force experienced by trapped beads near contact, as we will discuss later.

In many ways, the optical tolerances for forming a LOT resemble those for a conventional "point" optical tweezers, with the major exception being that LOTs are much less tolerant of longitudinal spherical aberration (LSA), corresponding to the edge rays of a converging beam crossing the optical axis behind (for LSA >0) the paraxial (center) rays [see Fig. 1(d)]. Off-axis aberrations in the optical train are nulled by careful centration and alignment of the optical elements.[15] Simple planoconvex elements are used throughout because they have nearly minimal LSA (provided their curved sides face the collimated beam and they are used at nearly infinite conjugate ratio), and their chromatic aberration is irrelevant for laser light. Nevertheless, each lens contributes a small amount of positive LSA to the beam. Often, the microscope objective contributes some (positive or negative) LSA as well, while corrected for LSA in visible light, their LSA is sometimes not nulled in the IR (termed spherochromaticity).

Because of LOTs' greater sensitivity to LSA, many optical trains and objectives that strongly trap particles when used in point traps will not stably trap particles when converted to a line trap (e.g., by scanning). LOTs with marginal LSA will generally be able to weakly trap bacteria and low index silica or PMMA microspheres, but will not stably trap higher index polystyrene particles. One remedy, if the objective is known to have negligible LSA, is to increase the focal length of the optical train to drive down its cumulative LSA. Another highly useful method (which we use in our instrument) is to slightly alter the refractive index of the immersion oil (sets of graded index oils are available from Cargille, Series A). Changing the oil index is equivalent to inserting a refractive slab into the high-NA converging beam approaching the trap [Fig. 1(d)]; even small changes can lead to significant differences in LSA and trapping strength. A corollary phenomenon, since the LSA of an oil-immersion objective depends on its focal position relative to the chamber cover slip, is that LOTs have a much narrower useful depth of focus than point traps. As expected, we have found high NA water immersion objectives to form excellent, focus independent LOTs (they also typically have a correction collar that enables the nulling of LSA). To avoid difficulties from immersion water evaporation in our heated samples, however,

we exclusively used an oil-immersion lens for this study.

High speed imaging using a CMOS camera

The last few years have seen the advent of relatively inexpensive (~$20 000), high speed digital cameras using complementary metal oxide semiconductor (CMOS)-based rather than charge-coupled device (CCD)-based detectors. The camera we use (Phantom 4, Vision Research) can acquire 512×512 images (noninterlaced, with 8 bit gray scale) at 1000 fps (frames per second). Since the corresponding data rate (256 Mbytes/s) is significantly higher than typical I/O interfaces, data are stored in an on-board random access memory (RAM) buffer and downloaded to a host computer at a lower rate (~10 Mbytes/s) when the buffer is filled. We find that the signal-to-noise ratio and dynamic range of the images from our camera are comparable to the interline-charge transfer CCD-based video cameras typically used for bright field microscopy. The sensitivity of our CMOS detector is roughly one-half to one-third that of video CCD's in visible light, but the two detectors are nearly equivalent at the near infrared wavelengths we employ. CMOS cameras do have a somewhat larger pixel-to-pixel variations in gain and background, but this "fixed pattern noise" is readily eliminated by flat fielding if it poses a problem.

One feature of most CMOS cameras is that they can also collect images at even higher speeds when using a smaller, software selected detector area. For example, as our line tweezers image fits on a 128×128 pixel area of the detector, we can acquire images at more than 15 000 fps when that is desirable. One complication, however, is that the fields of view at different frame rates are not concentric. We mounted our camera on an *x-y* translation stage, to allow us to easily recenter the CMOS detector over the LOT image, to avoid modifying traps' delicate optical alignment. We also added custom-built relay optics between the microscope and camera to provide an adjustable magnification with this arrangement. This allows us to increase the number of camera pixels per trapped bead, which further improves the resolution of our particle tracking algorithm. To provide a large diffraction-limited field of view we used a pair of achromatic doublet lenses for the relay optics, due to their superior off-axis performance.

High-brightness Kohler laser illuminator

We determine the particle positions on our images using a brightness-weighted centroiding algorithm. The ultimate spatial resolution of such methods depends on the camera's signal to noise ratio and system magnification.[16] For illumination just short of detector saturation (which typically yields maximal, roughly 100:1 signal to noise ratios), resolution is inversely proportional to magnification. In this limit, halving the spatial resolution (by doubling the magnification) requires quadruple the luminous flux at the specimen. Moreover, in most applications it is desirable that the particles diffuse less than the spatial resolution during the exposure to avoid introducing statistical biases and dynamic error to the data.[17] In these cases, improving spatial resolution demands correspondingly shorter exposure times and thus even higher luminous flux.

A typical video microscopy system with a halogen lamp illuminator using an interline CCD video detector, a magnification of 100 nm/pixel, and exposure times of 0.1–1 ms can locate 1 μm microspheres to 6–8 nm standard deviation. The use of a noninterlaced camera doubles the signal and improves the resolution by $\sqrt{2}$ to roughly 4–6 nm. For reference, such particles in water diffuse ~10 nm during a 100 μs exposure. At a constant specimen illumination from a halogen lamp (i.e., at its maximum setting), increasing the magnification much beyond this point will result in lower signal to noise imaging that will exactly offset the benefit of the higher magnification (assuming the exposure time cannot be increased). Doing better than roughly 5 nm spatial resolution, when tracking rapidly diffusing microspheres, requires a light source with higher brightness than can be provided by an incandescent lamp.

Of course, the high resolution of centroiding algorithms is well known to the single-molecule (fluorophore) tracking community. There, spatial resolutions of 1 nm are commonly achieved.[18,19] In those applications, however, the experiment can be arranged such that the motion is slow, Brownian jiggling minimized, and long trajectories are not required. This allows the use of long camera exposure times without corresponding dynamic error.[17] For our application, microspheres' rapid Brownian diffusion and our interest in high speed dynamics preclude this elegant solution.

Lasers are the ultimate high brightness light sources, but their coherence and collimation present several challenges to using them as microscope illuminators.[20] Because of coherence, light scattered from each microsphere (or defects in the optical train) interferes with that from all the others. From a simple centroiding point of view, such interference fringes resemble a time-varying nonuniform background illumination which badly biases and correlates the particle positions. Moreover, since the illumination is essentially collimated, particle images possess a broad set of intense diffraction rings, a large depth of focus, and low optical resolution. We sought to develop a laser illumination source embodying the principles of Kohler illumination: equal intensity illumination at every point in the specimen plane from every direction within some conical solid angle. Moreover, we hoped to eliminate coherence effects (interference and speckle), allowing the resulting illuminator to be functionally equivalent to a conventional lamp illuminator, but with much higher brightness and providing the option of pulsed illumination to avoid heating and photodamage effects.

Our source is a multimode GaAlAs diode laser emitting up to 2 W of light (Spectra Diode Labs, SDL-2460, $\lambda = 808$ nm). To increase the mode content of the beam to that required for Kohler illumination, this light is passed through a multiple mode optical fiber.[20] Laser's emitter (1×100 μm^2 in size) is imaged onto the 200 μm diameter core of a 5 m long fiber having a large enough critical NA to collect the light (see Fig. 2). The use of connecterized fibers and fiber collimators makes for a simple and compact optical system, where a single folding mirror and input collimator

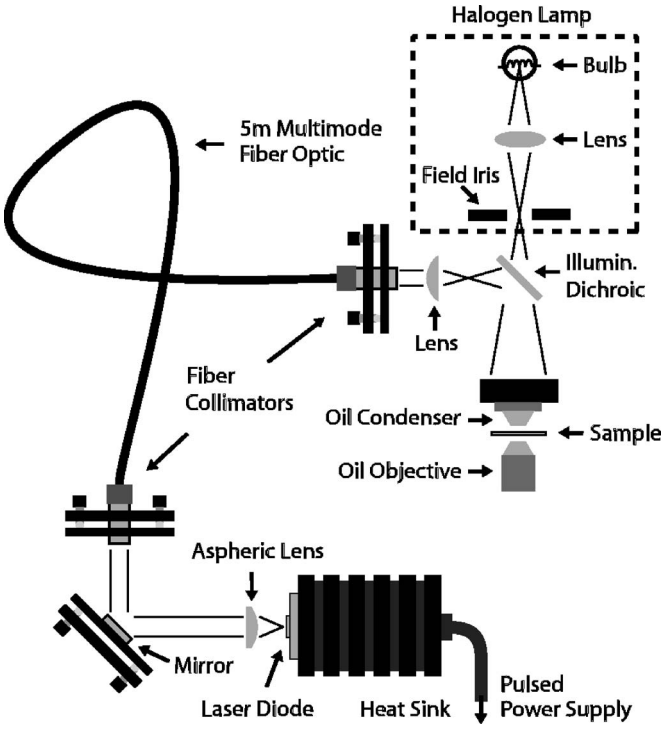

FIG. 2. Schematic of the IR illumination system. On the fiber input side, optics are arranged to image the diode junction onto a multimode fiber core with a magnification ≈1; kinematic mounts provide for the adjustment of beam centration and entrance angle. On the output side, the fiber core is imaged onto a plane conjugate to the microscope's field iris, which is itself conjugate to the specimen plane. The use of an IR illumination dichroic reflector that transmits white light facilitates alignment with the existing illuminator axis and rapid switching between laser and halogen illumination.

on kinematic mounts provide the four degrees of freedom needed for alignment.

A second fiber collimator and single planoconvex relay lens mounted on microscope's illumination stalk image the exit face of the fiber onto the specimen plane using microscope's high NA condenser lens (Fig. 2). To facilitate rapid switching between the IR and halogen illuminators, an IR reflective illumination dichroic is used. The relay lens is positioned so that its focal plane is the same distance from the condenser as the built-in field diaphragm.

The uniformity of the illumination across the field of view depends on the distribution of light across the fiber's exit face, and the NA of the illumination depends on the angular distribution of the light exiting the fiber. In the ideal Kohler case, both distributions would be uniform within circular spatial and angular apertures, respectively. Due to the optics of multimode fibers, each light ray proceeds down the fiber along a (piecewise linear) helical trajectory that "scrambles" the ray's azimuthal position. As a result, the distribution of light on the fiber's exit face and its angular distribution are azimuthally symmetric. In contrast, the radial distribution of the rays is not completely scrambled. The closest approach a ray makes to the fiber axis between reflections is preserved as it propagates down the fiber, meaning that the ray can only exit somewhere between that minimum radius and the edge of the core. In practice, imaging the laser emitter onto the center of the fiber core along its optical axis creates a smooth but nonuniform distribution of illumination with a maximum intensity near the fiber axis and a correspondingly peaked and narrow angular distribution. By intentionally misaligning the light entering the fiber, both in centration and incident angle, it is straightforward (through trial and error) to find arrangements with a relatively uniform distribution across the fiber exit face, a broad angular distribution, and power throughput comparable to the aligned case (typically 60% power transmission from the diode to the exit face). While the angular distribution can be quite broad, it cannot fill the NA of the fiber uniformly, since injecting rays near the fiber's critical limiting NA leads to their attenuation with a corresponding loss of transmission efficiency. For similar reasons, commercial "fiber scramblers" that controllably bend the fiber do not prove that useful either.

While scrambling light in an optical fiber alters the distribution and number of transverse optical modes, it does not significantly alter the spectrum or degree of coherence in the source. While our laser source has a complex transverse mode structure by itself, it generally operates at one or two longitudinal modes. As a result illumination by the fiber scrambled laser fills the microscope's field of view with high contrast speckles whose typical size (a micron or two) is set by the illumination NA. Imaging microspheres on such a speckle field is hopeless. Speckle can be eliminated by taking advantage of the fact that the wavelength of the source depends on both the diode current and temperature. When we rapidly pulse the diode, the slow rise and fall times of the diode current (and presumably its nonsteady temperature) cause the source to rapidly scan over a very large number of longitudinal modes. In practice, when we strobe the diode for durations less than ~200 μs, speckle and interference effects are essentially undetectable [see Fig. 1(c)]. We command a commercial current source to pulse the diode using a simple custom-built analog pulse generator circuit triggered by a strobe signal from our CMOS camera. This longitudinal mode sweeping via stroboscopic pulsing is far simpler and more effective than mechanical alternatives such as vibrating the optical fiber.

The final brightness of this arrangement is more than two orders of magnitude higher than obtained using the standard 100 W halogen illuminator. For bright field microscopy at a rather high magnification of 50 nm/pixel, we can saturate the CMOS detector using a stobe less than 5 μs in duration, which never reaches maximum diode current (the rise/fall time for our 2 A current source is roughly 5 μs). Such high brightness provides margin for enabling still higher magnifications or the use of contrast generation techniques such as phase-contrast or differential interference contrast (DIC) imaging. Because our trapping laser and illumination laser differ in wavelength by only 20 nm, the imaging dichroic we use to direct the trapping laser into the objective only transmits only ~20% of our illumination light, but that does not pose a problem given the illuminator's excess brightness.

Our illuminator compares favorably with more conventional stroboscopic illuminators, such as those based on xenon flash lamps. The instantaneous white-light brightness of such flash lamps can be tens of times brighter than a halogen lamp during a pulse lasting several microseconds, with a

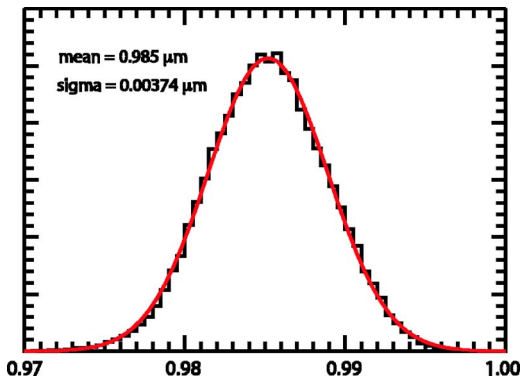

FIG. 3. (Color online) The probability distribution of the separation distance of a pair of microspheres irreversibly bound together. The distribution is Gaussian with a half width of 4 nm which represents the spatial resolution of our instrument.

typical maximum repetition rate of 100 Hz. Our laser illuminator can easily pulse at 10 kHz, has a higher peak brightness, has an adjustable pulse duration (allowing even higher illumination), and concentrates its light output at wavelengths where photodamage is unlikely. However, for video rate (<100 Hz) applications where white light is needed, a properly filtered xenon flash lamp might be a useful solution.

RESULTS

Instrumental resolution

The ultimate spatial resolution of our video-based particle tracking system depends on the camera's signal to noise ratio and the out-of-plane fluctuations of our trapped particles. In order to quantify the resolution, we tracked the motion of a trapped dimer particle (i.e., a pair of colloidal microspheres irreversibly stuck together). The center-to-center separation distance h of a dimer is fixed and should be roughly the spheres' mean diameter. Measuring its probability distribution $P(h)$ should give a delta function at its mean diameter. Instead we see a Gaussian-shaped distribution with a 4 nm half width, signifying our instrumental resolution (Fig. 3).

As described earlier, the contribution of the camera noise to our instrument resolution is inversely proportional to the system magnification. We can estimate its contribution to the total resolution by observing the effect on resolution of increasing the magnification. For our noninterlaced video microscopy system with a magnification of 50 nm/pixel and an exposure time of 5 μs, we can locate the center of a 1 μm particle to 1–2 nm standard deviation. Therefore, our camera noise contributes about 2–3 nm (in quadrature) to the 4 nm total error of our separation measurements. Further increasing the magnification has little effect on the overall resolution due to the remaining contribution from out-of-plane particle motion.

Since all optical traps have a finite trapping strength, out-of-plane fluctuations are unavoidable due to thermal activation. The extent of these out-of-plane (z directional) motions can be estimated from the brightness fluctuations of the trapped particles, which are about 3% in our system. We estimate that this brightness fluctuation corresponds to a

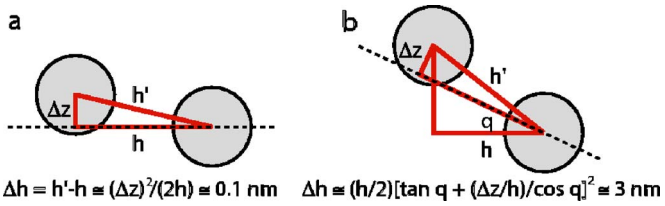

FIG. 4. (Color online) The uncertainty in our experimentally measured separation distance h due to out-of-plane fluctuations Δz (a) when the line optical tweezers, represented by the dotted line, is perfectly horizontal and (b) when it is tilted by some angle θ. Here h' is the actual separation. For the calculated values shown in (a) and (b), we assumed the spheres were near contact, $h'=2R$, with a radius of $R=490$ nm, $\Delta z=10$ nm, and $\theta=4°$.

10–15 nm standard deviation for the z motion. This is a significant improvement compared to scanned LOTs using a galvanometer-driven mirror,[5,7] which allow a few millisecond period, between scans, for the beads to freely diffuse. This can allow the spheres to travel more than 50 nm out of plane before they are pulled back to the line focus.

The extent at which our out-of-plane fluctuations effect the total resolution depends on the orientation of the LOT. Were our LOT perfectly aligned with the specimen plane, an out-of-plane fluctuation of 10–15 nm would contribute <0.1 nm to the spatial resolution of the separation distance [Fig. 4(a)]. If, however, the LOT were slightly tilted at an angle of about 4°, with respect to the optical specimen plane, then a 10–15 nm fluctuation in the z-direction would contribute a 3 nm uncertainty to our separation measurements [Fig. 4(b)]. This hypothesis is supported by a slight, systematic difference in the apparent brightness of the two particles in our trap. We have been so far unable to isolate and eliminate this optical tilt with the limited degrees of freedom of our optical train. We suppose that in a holographically generated LOT,[14] it would be straightforward to null both aberrations and tilt by modifying the computed hologram.[21] If this source of error were eliminated, it seems the remaining error due to centroiding could readily be reduced to the nanometer level by further increasing the optical magnification.

Diffraction-limited overlap effects

Particle tracking software can accurately locate the positions of objects in an image if the particles are well separated from each other. However, when two or more objects are near contact, their diffraction blurred edges overlap [Fig. 1(c)], causing the particle tracking algorithm to miscalculate objects' centroids. As a consequence, the particles can appear up to a couple hundred nanometers closer together or farther apart than they actually are.[22,23] To partially correct for this error, our centroiding algorithm determines the center of each microsphere after subtracting off the image of its neighboring particle.

Figure 1(c) shows a typical image of two microspheres in our optical trap. Each image is a two-dimensional representation of the intensity profile, I, at the camera. To first order, the total electric field, $\mathbf{E}$, at the camera equals the sum of electric fields, $\mathbf{E}_i$, scattered by the objects. In Fig. 1(c), $I \equiv |\mathbf{E}|^2 = I_1 + I_2 + 2\mathbf{E}_1 \cdot \mathbf{E}_2$, where $I_i \equiv |\mathbf{E}_i|^2$ is the intensity of the ith particle. As a first approximation, the algorithm ignores the interference term, $\mathbf{E}_1 \cdot \mathbf{E}_2$, and assumes that the image is a

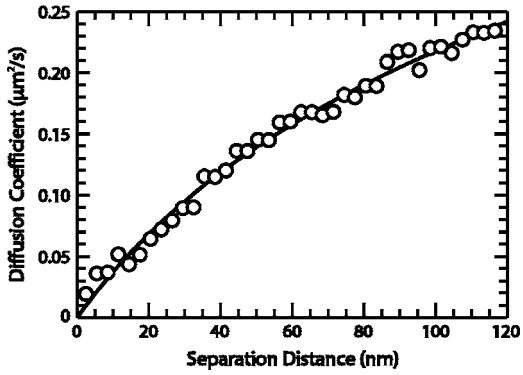

FIG. 5. The relative diffusion coefficient of two microspheres in our line optical trap as a function of their surface-to-surface separation distance, h. The experimentally measured diffusion coefficient (open circles) fits Eq. (1) with a shift of $h_0=120$ nm.

superposition of the intensity of each microsphere. Therefore, if we knew the intensity profile of the individual bead images, then we could correctly determine the centroid of either sphere by subtracting off the image of its neighbor. By assuming that the bead images are left-right symmetric, our algorithm estimates the brightness of bead's overlapping side by mirror reflecting its nonoverlapping side about its center.[22]

Of course, the problem is even more complicated than the one described above. Not only does our algorithm ignore the interference between single scattered fields, it also ignores the possibility of multiple scattering effects. Light scattered from one particle can refract through the other, altering its image and corresponding centroid. These effects will most likely increase with the refractive index of the microspheres.

To correct for any separation error due to these higher order effects, we self-consistently calibrate the measured particle separations using the known separation dependence of the diffusion coefficient of hydrodynamically coupled spheres. Near contact, the separation dependent diffusion coefficient $D(h)$ for a pair of spheres is well approximated by[24]

$$D(h)=\left[\frac{k_BT}{6\pi R\eta}\right]\frac{12(h/R)^2+8(h/R)}{6(h/R)^2+13(h/R)+2}, \qquad (1)$$

where T is the temperature, k_B is Boltzmann's constant, R is the radius of the microspheres, and η is the viscosity of the medium. To calibrate our instrument, we measured the separation distance h as a function of time t for several pairs of microspheres at a frame rate of 5000 fps. After separating h into narrow partitions, the relative diffusion coefficient $D_{\mathrm{exp}}(h)$ for that partition was determined[25] from the standard deviation of the change in h one frame (200 μs) later. We found that shifting our experimentally measured separation distances, h, by a constant offset, $h_0=120$ nm, results in D_{exp} agreeing with D (see Fig. 5). This suggests that higher order scattering effects near contact simply shift our measured separation distances by an approximately fixed amount. Stated another way, the nonsuperposition contributions lead to a significant shift of the relative image centroids, but this shift is a sufficiently slowly-varying function of particle separation that we may assume that it is a constant for separations less than 100 nm without significant error.

Measuring colloidal interactions and dynamics

From our measured set of separation distances h, we can extract a wealth of information about the underlying colloids. Unlike other microscopic methods that ultimately measure forces using the deflection of a spring (be it an AFM cantilever or a calibrated optical trap), we use the fluctuations in thermodynamic equilibrium to deduce the interaction energy. We obtain the pair potential energy $U(h)$ between colloids from their probability distribution $P(h)$ using the Boltzmann relation $P(h)\propto\exp[-U(h)/k_BT]$.[5] The time dependence of h is also obtained which allows study of the microsphere diffusive or binding kinetics. For colloidal systems with reversible binding interactions, $h(t)$ contains bound state lifetime information[8] (i.e., durations of time where the beads are stuck together). Unlike many biophysical measurements with AFM and optical tweezers force clamps[26] which apply a large bias tension to the molecular construct, our instrument can operate at negligible applied force.

The potential energy $U(h)$ obtained from inverting the Boltzmann distribution contains not only the microspheres' physical pair interaction but also contributions from the optical trap itself. The trap causes two separate contributions to the measured potential, one pushing them together, and the other pushing them apart. Because these two forces, described in the following section, have different functional dependences on trap length and laser polarization, we can arrange the trap such that the total optical force acting between the microspheres is nearly zero at contact, $h=0$. Because both optical forces vary somewhat slowly with separation, we find that the resulting optical potential is essentially flat for $0<h<80$ nm, with a typical force uncertainty of ±25 fN. (Alternatively, the trap can instead be adjusted to act as an ultralow force passive force clamp, having a small, roughly constant force <0.5 pN repulsion over the same separation range.) Beyond 80 nm, the residual optical forces push the microspheres together, effectively preventing them from ever getting more than about 150 nm apart. In this sense, our trap is optimized for the study of weak, short-ranged interactions; the particles spend much of their time near steric contact. The trap we describe here may not be suitable for studying interactions or molecular bridges much longer than about 100 nm.

In general to isolate the physical pair potential of interest, residual trap-induced interactions, if any, must be subtracted. A variety of methods for doing this subtraction has been developed and are described in detail in the literature. The easiest is to measure the total interaction potential for two optically and geometrically identical systems where the potential of interest is turned "on" and "off." Taking the difference of the two potentials removes all contributions due to the trap.[4,6,22] A second approach is to measure the potential as a function of trap power and extrapolate the results to zero trap power.[5] Alternatively, for long-ranged measurements (i.e., $h>500$ nm), the trap contribution can be computed from the single particle trap potential and subtracted.[7]

For the short-ranged potentials in our instrument this subtraction is almost unnecessary, as the forces are nulled near contact. In practice, we prepare a sample with optically identical microspheres which do not have a long range inter-

action. We iteratively measure the interaction of these spheres and adjust the line trap length, until a null is achieved. We then fit this control potential to a smooth function (outside of the repulsion near contact) to quantify the residual optical force. This fit is then subtracted from the physical colloidal interactions of interest, to remove the optical forces. While earlier studies[4,6,22] used a complicated phenomenological function, for this study a simple linear fit was performed to the control data and then subtracted from the measured potentials.

Once the optical forces have been removed, it is common practice to fit a model potential $U_m(h)$ to the data. To account for our instrument's finite spatial resolution, we first convert the model into a probability distribution using the Boltzmann relation, $P_m(h) \propto \exp[-U_m(h)/k_BT]$, numerically convolve it with a Gaussian kernel to simulate our instrumental resolution, and then convert it back to a potential by taking the logarithm.[5] In our system, we use a Gaussian blurring kernel with a standard deviation of 4 nm. This numerical blurring means that the fit curves are usually not available in closed analytic form; fortunately many least-squares fitting packages are now able to fit numerically generated curves.

Optical interactions

As we found in an earlier study,[5] one optical contribution to the measured interaction potential is caused by the trap exerting a time-averaged force along the particles' line of centers. For a perfectly harmonic trap, with a spring constant k, the resulting force pushing the microspheres together is also harmonic depending on their separation, that is, $U_1(h) \approx k(h+2R)^2/2$ and is independent of where the two particles' center of mass is in the trap. In a longer trap we used in the earlier studies, we found that the pair potential $U_1(h)$ accurately described the data when $h > 500$ nm, with a spring constant corresponding to that of the single-particle trapping potential along the line. Decreasing the length of our line optical tweezers should increase k and U_1 quadratically, because both trap shape (i.e., gradient of normalized intensity along the line) and the amount of optical power intercepted by the particle (i.e., trap strength) are inversely proportional to trap length.

A second optical contribution to the measured interaction potential, also described in our earlier study,[5] is less well understood. Subtracting the contribution of $U_1(h)$ from interaction data (using a quadratic fit) left a residual repulsion, $U_2(h)$ with a monotonic, roughly exponential form and a maximum range of $h \approx 500$ nm, which was linearly proportional to laser power. When trapping laser's **E** vector was parallel to line trap's long axis, the repulsion was about one-third as strong as when perpendicular, but had a similar h dependence. Since $U_2(h)$ is unrelated to trap shape, it should increase only linearly in strength when the line trap length is reduced. It is the different trap length dependences of U_1 and U_2 that allow us to null them by adjusting the trap length.

We conjecture that the repulsion $U_2(h)$ is due to radiation pressure from the light scattered off each sphere pushing away the other sphere. This hypothesis is qualitatively consistent with interaction's repulsive character, power proportionality, and the polarization sensitivity (more light is scattered in the plane perpendicular to **E**). Calculating such interactions directly is challenging given the coupling of the spheres' optical near fields and the low symmetry of the problem. Indeed, the interactions or "optical binding" of colloidal particles in intense optical fields is an area of current research.[27–29] Early work by Burns *et al.*[27] found strong long-ranged periodic interactions, which were hypothesized to be due to coherent optical frequency dipole-dipole interactions. Similar dipole-dipole interactions may contribute to our short-range optical repulsion; the absence of periodic interactions from our measurements[5] is presumably due to geometric differences from the instrument of Burns *et al.*.

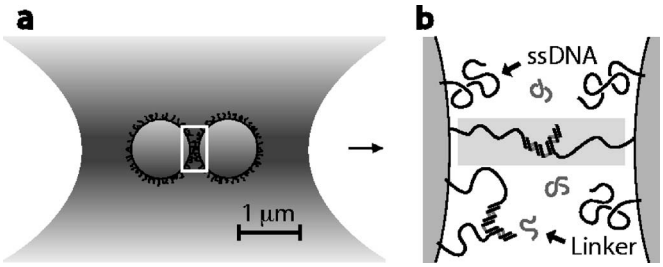

FIG. 6. (a) represents two microspheres trapped in the focal plane of a line optical tweezers. (b) shows microsphere surfaces chemically grafted with oligonucleotides, *s* (sequence: 5′-ACTTAACTACAGCATTATCAGTCT CCGAGGCCCATTGA TTCACACACGTCT**AACTTGAAATCTCT**-3′). Linker oligonucleotides (sequence: 5′-AGAGATTTCAAGTTCAGAG ATTTCAAGTT-3′) can bridge between microspheres (shaded box) after hybridizing with the terminal 14 bases of *s* (bold sequence).

Colloidal interactions due to DNA molecular bridges and micellar depletion

To demonstrate our instrument's ability to measure nanoscale interactions and kinetics, we present data for two systems. The first consists of two colloidal microspheres with single-stranded DNA grafted to their surface that can transiently bridge the spheres together.[30] The second system consists of charge stabilized microspheres with a weak attractive interaction due to the micellar depletion interaction.[31]

Research groups have been grafting DNA constructs to colloids and nanoparticles for nearly a decade.[30,32–34] The chemical specificity of DNA has been used to program the interactions between particles and surfaces, to drive colloidal aggregation,[34] crystallization,[30] and form self-assembled clusters.[33] Being limited to the length of the DNA, the interactions in these systems are short ranged, typically less then 50 nm; their temperature tunability makes them ideally suited for our apparatus. Directly measuring their pair interaction potential and binding kinetics should help understand the complex time- and temperature dependent phase behaviors these suspensions display.

Figure 6 shows our DNA adhesion system, consisting of 0.98 μm diameter carboxylate modified polystyrene microspheres in an aqueous buffer (10 mM tris, pH=8.0, 100 mM NaCl), each labeled with identical DNA oligonucleotides. The high salt concentration screens out electrostatic interactions to the point that the bead surfaces can come into steric contact. The ends of the DNA strands can then bridge the

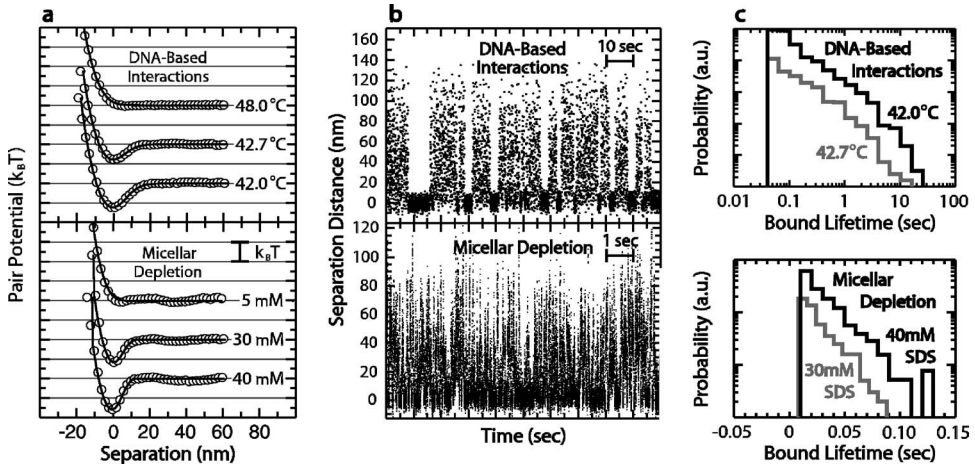

FIG. 7. Interaction and kinetics of our two colloidal adhesion systems: DNA bridging (top row) and micellar depletion (bottom row) (a) Pair potential energy between two microspheres, in k_BT units, with model fits described in the text (curves). Separation here is defined relative to the potential minimum. (b) shows the separation trajectory (distance vs time) for two trapped microspheres, with DNA bridging, for 100 s, $T=43.0\ ^\circ C$ (top) or with SDS micelles, 10 s (bottom). The microspheres are alternately bound or diffusing the width of the trap, with rather long bound lifetimes in the DNA case. (c) shows double logarithmic probability distributions of binding lifetime, for the DNA system at two different temperatures (top) or semilogarithmic distributions of binding lifetime in the depletion system.

microspheres together via the reversible hybridization of "linker" strands in solution [Fig. 6(b), shaded box], inducing a short-ranged attraction between them. DNA thermodynamic models predict that these bridges become unstable above $\sim 46\ ^\circ C$.[35] The hybridizable ends are separated from the microsphere surface by a spacer consisting of single-stranded DNA, which sets the range of the interaction. All DNA sequences were designed to have low secondary structure and minimal sequence repetition with melting temperatures for all nondesigned conformations below 25 °C. Compared to the particles reported in an earlier study,[8] these particles were optimized to be sterically stable at lower DNA density ($\approx$2000 molecules/sphere). This was accomplished by covering the colloidal surfaces with grafted polyethylene glycol (PEG); the oligonucleotides are covalently linked to the ends of the PEG chains.[36]

For comparison, we also studied a micellar depletion system, consisting of 0.98 μm diameter polystyrene sulfate in low salt buffer (10 mM tris, pH=8.0, 20 mM NaCl) with varying amounts of added sodium dodecyl sulfate (SDS). When added above the critical micellar concentration (CMC 7 mM), the excess SDS forms spherical micelles with a hydrodynamic diameter of about 4–5 nm. Exclusion of these micelles from the space between the microspheres leads to a weak entropic attraction, with a range equal to the diameter of the micelle.

We directly measured the microsphere pair interactions and dynamics of both systems following the procedure described earlier. The upper panel of Fig. 7(a) displays the DNA interaction potential energy as a function of separation and temperature. The data indicate a short-range attraction that decreases in strength as the temperature increases, vanishing by 46 °C, along with a soft, temperature independent repulsion near contact. The pair interactions in our system consist of a temperature dependent attraction due to dynamically forming and breaking DNA bridges between the microspheres, and a nearly temperature independent entropic repulsion due to compression of the grafted DNA.[8] Though the contour length of our DNA is $\sim$40 nm, its effective length will be smaller since the persistence length of single stranded DNA is $\sim$2.5 nm at 100 mM NaCl.[37] If we model the DNA as a tethered Gaussian coil, the mean length, L, is around 15 nm. The attractive part of the total interaction has a range of $\approx 2L=30$ nm, where h is the surface-to-surface separation between the spheres. DNA on one sphere colliding with the opposing sphere produces a repulsion with range $\approx L$. Thus, the expected attractive well width is of the order L in accordance with our measurements. A quantitative model based on these principles is described in an earlier publication.[8] It can fit the observed interaction quantitatively [Fig. 7(a), curves], using only the known thermodynamic[35,37] and structural parameters of single-stranded DNA.

Similarly, the bottom panel of Fig. 7(a) shows the micellar depletion interaction, with a width consistent with the scale of a SDS micelle, broadened slightly by our instrumental resolution. The unblurred interaction model is the Asakura-Oosawa depletion potential[38] using an effective micelle radius and volume fraction that corrects for the electrostatic repulsion between the charged micelles and microspheres, as described in Ref. 5. While the width of the potential is comparable to our limiting instrumental resolution, fitting the data yields an effective diameter for the micelles of $\approx$5 nm and a concentration consistent with the added SDS.

To study the binding dynamics in detail, we examined the time-varying separation between the two microspheres in our trap [Fig. 7(b)]. In the DNA system, (top panel), the microspheres are alternately bound by DNA bridges ($h<2L$) or unbound and diffusing to the width of the optical trap. The abrupt transitions between the two behaviors are the consequence of discrete molecular binding events. The expected lifetime of the DNA bridges and microspheres' diffusive escape time are both $\sim$10 ms. While a subset of

bound states are that short lived, many other bound states last up to tens of seconds. In an earlier study, we found these long-lived events to have a roughly power-law distribution $P(t) \sim t^b$ with $b \approx -1.5$ at all temperatures. In this study, we find clear deviations from this form, with the lifetime histogram showing a clear curvature on a double logarithmic plot [Fig. 7(c), top]. Since the only change here is the reduced DNA density, this demonstrates that the power-law behavior is a high-DNA density effect, and thus presumably related to multiple DNA bridged states. For comparison, the kinetics of the micellar system are much faster [Fig. 7(b), bottom, expanded scale] and have the exponentially distributed lifetimes expected for a simple two-state system, i.e., the histogram is a straight line on a semilogarithmic plot [Fig. 7(c), bottom]. The micellar system demonstrates the ability of our system to follow fast (tens of microseconds) binding reactions and confirms that the unusual, nonexponential kinetics seen in the DNA bridge case is not due to microsphere diffusion or other instrumental artifacts.

DISCUSSION

Other similar approaches for measuring quasistatic colloidal forces (TIRM or RIM) track the Brownian fluctuations of a single large ($5-10\ \mu$m) microsphere near a flat wall.[31,39] These Brownian fluctuation based approaches match or exceed the force sensitivity ($\ll 1$ pN) of comparable, time-averaged spring-based approaches (e.g., AFM cantilevers and optical tweezers laser deflection). The relative diffusion coefficient of our 2 μm sized probes, however, is more than an order of magnitude higher than that of such large tracers or cantilevers, allowing us to follow faster kinetics and collect higher statistical power in less time. Our method has the additional advantage that both surfaces are colloidal, can be made identical, and can be prepared and quantified using the same techniques (such as flow cytometry). Lastly, since both of our spherical probes tumble randomly in the trap, we can easily ensemble average the surface energy over both spheres' surfaces, rather than sampling a single small area of a flat wall.

Strictly from a particle tracking point of view, researchers have generally had to choose between two very different types of approaches: image analysis approaches, such as video particle tracking (VPT),[16] and laser-deflection particle tracking (LDPT).[26] LDPT readily achieves spatial resolutions of 0.1 nm, with bandwidths of 100 kHz or more, allowing it to follow very rapid nanoscale motion. As we have seen, VPT of rapidly diffusing objects typically does no better than 5 nm resolution with 60 Hz bandwidth. While obviously inferior from a resolution and bandwidth point of view, VPT has been widely adopted due to other factors, primarily ease of setup, calibration and use, low cost, and its ability to simultaneously track large numbers of tracers. In this context, our CMOS camera/laser illumination system is itself a breakthrough. It retains the capabilities and versatility of VPT, but by virtue of much faster electronics and higher illumination levels can simultaneously achieve resolutions and bandwidths (1 nm at 10 kHz) approaching that of LPDT. This combination of features has already proved key to cell microrheology measurements requiring multiple particle tracking.[40] For laboratories already using VPT but requiring superior resolution or bandwidth, our CMOS camera/illuminator would be a straightforward "upgrade."

The telegraphic nature of the trajectory data in Fig. 7(b) clearly shows that our LOT instrument has the spatial and temporal resolutions to follow discrete single-molecular binding and unbinding events. Compared to assays which study a molecular bridge construct between a trapped particle and the chamber cover slip or a micropipette, "two-trapped-bead" approaches are far less sensitive to high-frequency mechanical vibration and long time drift of the sample stage. Recently, Greenleaf *et al.* described an elegant double optical trap instrument[41] which uses LDPT and forms a passive force clamp using trap anharmonicity. Like our instrument, it is well suited to measuring the length fluctuations of short molecular constructs, under tensions of order 10 pN. Our instrument has a complementary role, being designed to study extremely short (<50 nm) molecular constructs under tensions of $0-1$ pN. Rather than using optical tweezers to study the fascinating mechanochemistry of single molecules in response to force, we will study the equilibrium, thermally accessible states, and conformational changes of these constructs. Indeed, there are a wealth of weakly interacting protein/DNA complexes whose binding has not been characterized in detail. Moreover, there are interesting problems in cell biophysics, for example, the formation and maintenance of neuronal and immunological synapses, which are governed by the gentle adhesion of small numbers of very weak ligand-receptor pairs. Our instrument is ideally suited to the study of such problems.

SUMMARY

In conclusion, we have demonstrated a line optical tweezers based method for measuring the equilibrium forces and dynamics between pairs of colloidal microspheres with few-nanometer resolution. This instrument is ideally suited to the measurement of a variety of extremely weak interactions due to colloidal forces. The instrument has been used to investigate the weak adhesion induced by the dynamic hybridization of grafted DNA brushes in the absence of an external force. Similarly, future measurements should elucidate a number of important biophysical problems that are mediated by single weakly bound complexes or small ensembles of weak ligand-receptor pairs. This versatility will allow our instrument to seamlessly bridge from the colloidal scale to the single-molecular scale.

ACKNOWLEDGMENTS

The authors thank Daniel Chen, David Grier, Mohammad Islam, Anthony Kim, Vinothan Manoharan, J.C. Meiners, Eric Weeks, and Arjun Yodh for useful and stimulating discussions. This work was supported by NSF-MRSEC and NSF-DMR.

[1] A. Ashkin, J. M. Dziedzic, J. E. Bjorkholm, and S. Chu, Opt. Lett. **11**, 288 (1986).
[2] K. Sasaki, M. Koshioka, H. Misawa, N. Kitamura, and H. Masuhara, Opt. Lett. **16**, 1463 (1991).

[3] L. P. Faucheux, L. S. Bourdieu, P. D. Kaplan, and A. J. Libchaber, Phys. Rev. Lett. **74**, 1504 (1995).
[4] R. Verma, J. C. Crocker, T. C. Lubensky, and A. G. Yodh, Phys. Rev. Lett. **81**, 4004 (1998).
[5] J. C. Crocker, J. A. Matteo, A. D. Dinsmore, and A. G. Yodh, Phys. Rev. Lett. **82**, 4352 (1999).
[6] K. H. Lin, J. C. Crocker, A. C. Zeri, and A. G. Yodh, Phys. Rev. Lett. **87**, 088301 (2001).
[7] M. Brunner, J. Dobnikar, and H. H. von Grunberg, Phys. Rev. Lett. **92**, 078301 (2004).
[8] P. L. Biancaniello, A. J. Kim, and J. C. Crocker, Phys. Rev. Lett. **94**, 058302 (2005).
[9] R. Nambiar, A. Gajraj, and J. C. Meiners, Biophys. J. **87**, 1972 (2004).
[10] L. P. Faucheux, G. Stolovitzky, and A. J. Libchaber, Phys. Rev. E **51**, 5239 (1995).
[11] R. Nambiar and J. C. Meiners, Opt. Lett. **27**, 836 (2002).
[12] S. A. Tatarkova, A. E. Carruthers, and K. Dholakia, Phys. Rev. Lett. **89**, 283901 (2002).
[13] J. E. Curtis and D. G. Grier, Opt. Lett. **28**, 872 (2003).
[14] Y. Roichman and D. G. Grier, Opt. Lett. **31**, 1675 (2006).
[15] E. Hecht, *Optics*, 3rd ed. (Addison-Wesley, Reading, MA, 1998).
[16] J. C. Crocker and D. G. Grier, J. Colloid Interface Sci. **179**, 298 (1996).
[17] T. Savin and P. S. Doyle, Biophys. J. **88**, 623 (2005).
[18] J. Gelles, B. J. Schnapp, and M. P. Sheetz, Nature (London) **331**, 450 (1988).
[19] A. Yildiz, J. Forkey, S. McKinney, T. Ha, Y. Goldman, and P. Selvin, Science **300**, 2061 (2003).
[20] B. Dingel and S. Kawata, Opt. Lett. **18**, 549 (1993).
[21] E. R. Dufresne, G. C. Spalding, M. T. Dearing, S. A. Sheets, and D. G. Grier, Rev. Sci. Instrum. **72**, 1810 (2001).
[22] R. Verma, J. C. Crocker, T. C. Lubensky, and A. G. Yodh, Macromolecules **33**, 177 (2000).
[23] J. Baumgartl and C. Bechinger, Europhys. Lett. **71**, 487 (2005).
[24] T. G. M. VanDeVen, *Colloidal Hydrodynamics*, 1st ed. (Academic, London, 1989).
[25] J. C. Crocker, J. Chem. Phys. **106**, 2837 (1997).
[26] K. C. Neuman and S. M. Block, Rev. Sci. Instrum. **75**, 2787 (2004).
[27] M. M. Burns, J.-M. Fournier, and J. A. Golovchenko, Science **249**, 749 (1990).
[28] N. K. Metzger, K. Dholakia, and E. M. Wright, Phys. Rev. Lett. **96**, 068102 (2006).
[29] N. K. Metzger, E. M. Wright, W. Sibbett, and K. Dholakia, Opt. Express **14**, 3677 (2006).
[30] A. J. Kim, P. L. Biancaniello, and J. C. Crocker, Langmuir **22**, 1991 (2006).
[31] D. L. Sober and J. Y. Walz, Langmuir **11**, 2352 (1995).
[32] C. A. Mirkin, R. L. Letsinger, R. C. Mucic, and J. J. Storhoff, Nature (London) **382**, 607 (1996).
[33] C. M. Soto, A. Srinivasan, and B. R. Ratna, J. Am. Chem. Soc. **124**, 8508 (2002).
[34] V. T. Milam, A. L. Hiddessen, J. C. Crocker, D. J. Graves, and D. A. Hammer, Langmuir **19**, 10317 (2003).
[35] J. J. SantaLucia, Proc. Natl. Acad. Sci. U.S.A. **95**, 1460 (1998).
[36] A. J. Kim, V. N. Manoharan, and J. C. Crocker, J. Am. Chem. Soc. **127**, 1592 (2005).
[37] M. C. Murphy, I. Rasnik, W. Cheng, T. M. Lohman, and T. Ha, Biophys. J. **86**, 2530 (2004).
[38] S. Asakura and F. Oosawa, J. Polym. Sci. **33**, 183 (1958).
[39] S. Biggs, D. C. Prieve, and R. R. Dagastine, Langmuir **21**, 5421 (2005).
[40] B. D. Hoffman, G. Massiera, K. M. VanCitters, and J. C. Crocker, Proc. Natl. Acad. Sci. U.S.A. **103**, 10259 (2006).
[41] W. J. Greenleaf, M. T. Woodside, E. A. Abbondanzieri, and S. M. Block, Phys. Rev. Lett. **95**, 208102 (2005).